Letter

Multipolar Fermi-surface deformation in a Rydberg-dressed Fermi gas with long-range anisotropic interactions

Yijia Zhou [1,2] Rejish Nath [3] Haibin Wu,[4,5] Igor Lesanovsky [1,6] and Weibin Li [1]

[1]*School of Physics and Astronomy and Centre for the Mathematics and Theoretical Physics of Quantum Non-equilibrium Systems, University of Nottingham, Nottingham NG7 2RD, United Kingdom*

[2]*Graduate School of China Academy of Engineering Physics, Beijing 100193, China*

[3]*Department of Physics, Indian Institute of Science Education and Research, Dr. Homi Bhabha Road, Pune 411008, Maharashtra, India*

[4]*State Key Laboratory of Precision Spectroscopy, East China Normal University, Shanghai 200062, China*

[5]*Collaborative Innovation Center of Extreme Optics, Shanxi University, Taiyuan 030006, China*

[6]*Institut für Theoretische Physik, University of Tübingen, 72076 Tübingen, Germany*

(Received 5 May 2021; accepted 7 December 2021; published 20 December 2021)

We study theoretically the deformation of the Fermi surface (FS) of a three-dimensional gas of Rydberg-dressed ^{6}Li atoms. The laser dressing to high-lying Rydberg D states results in angle-dependent soft-core-shaped interactions whose anisotropy is described by multiple spherical harmonics. We show that this can drastically modify the shape of the FS and that its deformation depends on the interplay between the Fermi momentum k_F and the reciprocal momentum $\bar{k}$ corresponding to the characteristic soft-core radius of the dressing-induced potential. When $k_F < \bar{k}$, the dressed interaction stretches a spherical FS into an ellipsoid. When $k_F \gtrsim \bar{k}$, complex deformations are encountered which exhibit multipolar characteristics. We analyze the formation of Cooper pairs around the deformed FS and show that they occupy large orbital angular momentum states (p, f, and h wave) coherently. Our study demonstrates that Rydberg dressing to high angular momentum states may pave a route toward the investigation of unconventional Fermi gases and multiwave superconductivity.

DOI: 10.1103/PhysRevA.104.L061302

Introduction. Fermi surfaces (FSs), describing the occupation of momentum space by fermions, lie at the heart of Fermi liquid theory [1]. Though typically being a sphere in free space, FSs can be deformed by anisotropic two-body interactions, resulting in novel physics, manifesting in the nematic phase [2] and the Pomeranchuk instability [3]. Quantum simulators based on ultracold atoms provide a flexible platform for realizing Fermi gases with controllable FS [4]. Spherical FSs have been observed in free [5] and weakly interacting gases [6]. The spherical symmetry can be broken by anisotropic dipole-dipole interactions [7–13], and the deformation of the FS from a sphere to ellipsoid [14–22] has been observed in polarized dipolar gases [23].

A newly emerged approach to creating long-range interactions is so-called Rydberg dressing [24–29]: Using off-resonant lasers, the strong van der Waals interaction between electronically high-lying Rydberg atoms [30–32] is mapped to the ground state, yielding an effective interaction between dressed atoms that possesses a characteristic "soft-core" shape. The radius $\bar{R}$ at which the soft core occurs [25] and the potential shape can be tuned by dressing to different Rydberg states [33–37]. Generically, the collective behavior of the atomic gas is strongly impacted by the soft-core interaction [25,27,35,38]. In particular, the stability of elementary excitation and the emergence of supersolidity is connected to $\bar{R}$. So far experimental and theoretical studies have mostly focused on spin [39–41] and bosonic systems [25–29,42–44]. In a recent experiment [45], dressing of the fermionic ^{6}Li atoms to Rydberg P states was demonstrated, which indeed highlighted new opportunities for the exploration of correlated many-body phases with Rydberg-dressed fermions [46–50].

In this work, we study the FS deformation of a spin-polarized, zero-temperature gas of ^{6}Li atoms through Rydberg dressing. We find that the emerging long-range attractive two-body interaction $V(\mathbf{r})$ combines monopole, dipole, and quadrupole components [Fig. 1(a)], when dressing the ground-state atoms to a high-lying Rydberg D state. In momentum space, the interaction $\tilde{V}(\mathbf{k})$ is largest at around $k(\theta) = 5\pi/3R(\theta)$ with $R(\theta)$ being the angle-dependent soft-core radius [Fig. 1(b)]. When the Fermi momentum becomes larger than the minimum $k(\theta)$, the FS is strongly deformed and gains multipolar symmetries. We show that this deformation is accompanied by the formation of Cooper pairs, where p-, f-, and h-wave pairings coexist coherently when multipolar FS deformation occurs. The p- and f-wave pairings are key to the superfluidity of ^{3}He [51,52] and unconventional superconductors as shown in Ref. [53], while h-wave pairing has, to the best of our knowledge, not been identified in any other system. Our work shows that Rydberg-dressed fermions provide a tunable quantum simulator for investigating novel FS deformation and nontrivial pairing states.

Anisotropic Rydberg-dressed interaction. In our setting, each Li^6 atom consists of the electronic ground state $|g\rangle = |2S_{1/2}\rangle$, intermediate state $|e\rangle = |2P_{3/2}\rangle$, and Rydberg state $|r\rangle = |nD_{5/2}\rangle$ (n denotes the principal quantum number), as shown in Fig. 2(a). A probe and a control laser couple the

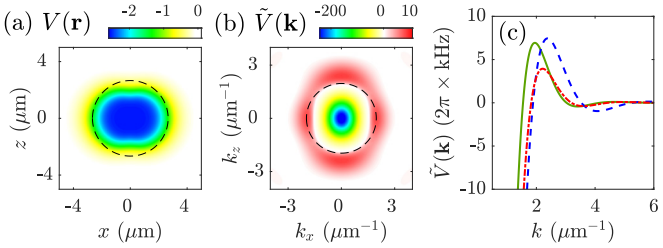

FIG. 1. Anisotropic soft-core interaction through Rydberg dressing. (a) Angular dependence of the attractive, soft-core interaction $V(d,\theta)$ in the xz plane. The interaction is stronger (weaker) along the $x(z)$ axis. The dashed line shows the circle whose radius is $\bar{R}$. (b) The Fourier transformed potential $\tilde{V}(\mathbf{k})$ is attractive at small momentum and becomes repulsive around $\bar{k}\approx 5\pi/(3\bar{R})$ (dashed line). (c) Profile of $\tilde{V}(\mathbf{k})$ cuts along the polar angle $\theta_k=0$ (blue dashed), $\pi/2$ (green solid), and π (red dash-dot). We consider $n=40$, $V_0\approx -2\pi\times 2.53$ kHz, and $\delta=-2\pi\times 40$ MHz. The energy unit in panels (a) and (b) is $2\pi\times$ kHz. See text for details.

$|g\rangle\leftrightarrow|e\rangle$ and $|e\rangle\leftrightarrow|r\rangle$ transitions. This coupling is described by the single-atom Hamiltonian $\hat{H}^{(1)}=\delta_p|e\rangle\langle e|+(\delta_p+\delta_c)|r\rangle\langle r|+(\Omega_p/2)(|g\rangle\langle e|+|e\rangle\langle g|)+(\Omega_c/2)(|e\rangle\langle r|+|r\rangle\langle e|)$, where Ω_p (Ω_c) and δ_p (δ_c) are Rabi frequency and detuning of the probe (control) laser, respectively. The state $|e\rangle$ can be adiabatically eliminated, provided that $|\delta_p|\gg|\Omega_p|$, $|\Omega_c|$, and $|\delta_c|$. This leads to an effective Hamiltonian, $\hat{H}_{\rm e}^{(1)}\approx\Delta|r\rangle\langle r|-\Omega/2(|g\rangle\langle r|+|r\rangle\langle g|)$, with the effective detuning $\delta\approx\delta_p+\delta_c-(\Omega_c^2-\Omega_p^2)/(4\delta_p)$ and Rabi frequency $\Omega=\Omega_p\Omega_c/(2\delta_p)$.

When excited to the Rydberg state, two atoms interact through the angular-dependent van der Waals (vdW) interaction $V_{\rm vdW}(d,\theta)=C_6(\theta)/d^6$, where $C_6(\theta)$ is the dispersion coefficient, $d=|\mathbf{r}-\mathbf{r}'|$ is the distance between the atoms (locating at $\mathbf{r}$ and $\mathbf{r}'$), and θ is the angle between the atoms and quantization z axis [see Fig. 2(b)]. We obtain the two-atom Hamiltonian, $\hat{H}^{(2)}=\hat{H}_{\rm e}^{(1)}(\mathbf{r})+\hat{H}_{\rm e}^{(1)}(\mathbf{r}')+V_{\rm vdW}(d,\theta)|rr\rangle\langle rr|$. In $|nD_{5/2},5/2\rangle$ states of ^{6}Li atoms, the dispersion coefficient can be expressed in terms of spherical harmonics $Y_{lm}(\theta)$ (l is an even number)

$$C_6(\theta)=\mathcal{C}_0Y_{00}(\theta)+\mathcal{C}_2Y_{20}(\theta)+\mathcal{C}_4Y_{40}(\theta), \tag{1}$$

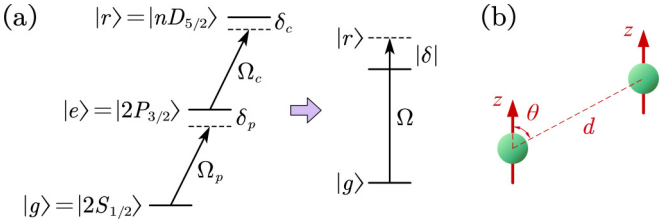

FIG. 2. Rydberg dressing. (a) Two-photon dressing scheme. The probe laser is far and blue detuned while the control laser is on resonance. The three-level system can be simplified to a two-level model by adiabatic elimination. The effective Rabi frequency is $\Omega=\Omega_p\Omega_c/(2\delta_p)$, and the effective detuning is $\delta=\delta_p+\delta_c-(\Omega_c^2-\Omega_p^2)/(4\delta_p)$. (b) Displacement between two atoms, and θ is the angle between the displacement and quantization axis.

which consists of monopole, dipole, and quadrupole components [54] with strength $[\mathcal{C}_0,\mathcal{C}_2,\mathcal{C}_4]=[-17.32,5.98,-0.076]\times10^{-17}n^{11}$ GHz μm^6 [55].

When $|\Delta|\gg|\Omega$, the ground-state atoms are weakly coupled to the Rydberg state, such that they experience a weaker, laser-dressed two-body interaction. The dressed interaction can be obtained through the conventional fourth-order perturbation calculation [25,56]. One can also derive the dressed interaction through the projection operator method [57]. We first define the two-atom ground-state subspace given by $\hat{P}=|gg\rangle\langle gg|$. The effective Hamiltonian in this subspace is

$$\hat{H}_{\rm eff}=\hat{P}\hat{H}\hat{P}-\hat{P}\hat{H}\hat{Q}\frac{1}{\hat{Q}\hat{H}\hat{Q}}\hat{Q}\hat{H}\hat{P}, \tag{2}$$

where $\hat{Q}=\hat{\mathbb{I}}-\hat{P}$ with $\hat{\mathbb{I}}$ being the identity operator. This results in the dressed interaction potential

$$V(d,\theta)=V_0\frac{R^6(\theta)}{d^6+R^6(\theta)}, \tag{3}$$

in which the soft-core radius $R(\theta)=\sqrt[6]{C_6(\theta)/2\delta}$ depends on the state- and angle-dependent dispersion coefficient $C_6(\theta)$, and the strength $V_0=\Omega^4/(8\delta^3)$. The detuning δ and the potential depth V_0 can be controlled by the dressing laser [55]. When $C_6(\theta)<0$ and $\delta<0$, the dressed interaction is attractive everywhere. Moreover, it is of cylindrical symmetry with respect to the z axis [Fig. 1(a)], as $C_6(\theta)$ has no dependence on the azimuth angle [as $m=0$ for all $Y_{lm}(\theta)$ of Eq. (1)].

Although $V(d,\theta)$ is attractive for all interparticle distance d, its Fourier transform, $\tilde{V}(\mathbf{k})$, is attractive when $k(\theta_k)$ is small and becomes positive when $k(\theta_k)>1.37\pi/R(\theta_k)$ [Fig. 1(b)]. It reaches the maximum around $k(\theta_k)\approx 5\pi/3R(\theta_k)$ [Fig. 1(c)]. As we will show later, the positive region turns out to be important in determining the ground state of the Fermi gas. For convenience, we will use $\bar{k}\approx 5\pi/3\bar{R}$ as the characteristic momentum, where $\bar{R}=R(\pi/2)$ is the soft-core radius along the x axis [Fig. 1(a)]. $\tilde{V}(k)$ depends on the modulus $|k|$ as well as on the polar angle (in k space) θ_k. This is in contrast to dipolar interactions whose Fourier transform is solely a function of the polar angle [7,19].

Modeling the Rydberg-dressed ^{6}Li *gas.* Our system is a three-dimensional (3D) homogeneous gas of N dressed ^{6}Li atoms, whose Hamiltonian is given by

$$\begin{aligned}H=&\int d\mathbf{r}\,\hat{\psi}^\dagger(\mathbf{r})\left[-\frac{\hbar^2}{2m}\nabla^2-\mu\right]\hat{\psi}^\dagger(\mathbf{r})\\&+\iint d\mathbf{r}d\mathbf{r}'\,\hat{\psi}^\dagger(\mathbf{r})\hat{\psi}^\dagger(\mathbf{r}')V(d,\theta)\hat{\psi}(\mathbf{r}')\hat{\psi}(\mathbf{r}),\end{aligned} \tag{4}$$

where the operator $\hat{\psi}(\mathbf{r})$ annihilates a Fermion with mass m at position $\mathbf{r}$. The first line of the above Hamiltonian gives the usual kinetic energy and chemical potential μ. The second line describes the interaction between two Fermions at positions $\mathbf{r}$ and $\mathbf{r}'$ via the soft-core potential. Using the plane-wave basis, the Hamiltonian can be re-expressed as

$$\begin{aligned}H=&\int\frac{d^3\mathbf{k}}{(2\pi)^3}\left(\frac{\hbar^2|\mathbf{k}|^2}{2m}-\mu\right)\hat{a}_{\mathbf{k}}^\dagger\hat{a}_{\mathbf{k}}\\&+\iiint\frac{d^3\mathbf{k}}{(2\pi)^3}\frac{d^3\mathbf{k}'}{(2\pi)^3}\frac{d^3\mathbf{q}}{(2\pi)^3}\hat{a}_{\mathbf{k}+\mathbf{q}}^\dagger\hat{a}_{\mathbf{k}'}^\dagger\tilde{V}(\mathbf{q})\hat{a}_{\mathbf{k}'+\mathbf{q}}\hat{a}_{\mathbf{k}},\end{aligned} \tag{5}$$

where $\hat{a}_{\mathbf{k}} = \int d^3\mathbf{r}\hat{\psi}(\mathbf{r})e^{-i\mathbf{k}\cdot\mathbf{r}}$ ($\hat{a}^\dagger_{\mathbf{k}} = \int d^3\mathbf{r}\hat{\psi}^\dagger(\mathbf{r})e^{i\mathbf{k}\cdot\mathbf{r}}$) is the annihilation (creation) operator of a Fermion with momentum $\mathbf{k}$.

To understand the impact of the anisotropic interaction on the many-body physics, we study the ground state of the system within the Hartree-Fock-Bogoliubov (HFB) approach [21,58]. Assuming pairing occurs between particles with momentum $\mathbf{k}$ and $-\mathbf{k}$, this allows to write down the BCS wave function $|G\rangle_{\rm BCS} = \prod_{\mathbf{k}}(u_{\mathbf{k}} + v_{\mathbf{k}}\hat{a}^\dagger_{\mathbf{k}}\hat{a}^\dagger_{-\mathbf{k}})|0\rangle$. The ground state is determined by the approximate HFB Hamiltonian,

$$H_{\rm HFB} = \int \frac{d^3\mathbf{k}}{(2\pi)^3}\,\xi_{\mathbf{k}}\hat{a}^\dagger_{\mathbf{k}}\hat{a}_{\mathbf{k}} + \left[\Delta(\mathbf{k})\hat{a}^\dagger_{\mathbf{k}}\hat{a}^\dagger_{-\mathbf{k}} + \text{H.c.}\right], \qquad (6)$$

where $\xi_{\mathbf{k}} = \varepsilon_k + U_e(\mathbf{k}) + U_d - \mu$ with $\varepsilon_k = \hbar^2|\mathbf{k}|^2/2m$ being the kinetic energy of free fermions. The Hartree energy $U_d = N\tilde{V}(0)$ is a constant and can be absorbed into the chemical potential. Both the Fock energy $U_e(\mathbf{k}) = -\sum_{\mathbf{k}'}\tilde{V}(\mathbf{k}-\mathbf{k}')\langle\hat{a}^\dagger_{\mathbf{k}'}\hat{a}_{\mathbf{k}'}\rangle$ and the gap function $\Delta(\mathbf{k}) = \sum_{\mathbf{k}'}\tilde{V}(\mathbf{k}-\mathbf{k}')\langle\hat{a}_{-\mathbf{k}'}\hat{a}_{\mathbf{k}'}\rangle$ depend on $\tilde{V}(\mathbf{k})$. The shape of the interaction, i.e., $\tilde{V}(-\mathbf{k}) = \tilde{V}(\mathbf{k})$, implies $U_e(-\mathbf{k}) = U_e(\mathbf{k})$ and $\Delta(-\mathbf{k}) = -\Delta(\mathbf{k})$. In the absence of two-body interaction, $\tilde{V}(\mathbf{k}) = 0$, one obtains a spherical FS of radius $k_F = (6\pi^2\rho)^{1/3}$ (ρ is the real space density) in momentum space, where the density distribution is $\tilde{\rho}_0(\mathbf{k}) = \Theta(|k_F - \mathbf{k}|)$ in the ground state with $\Theta(\cdot)$ to be the Heaviside function. As the variational parameter $u_{\mathbf{k}}$ and $v_{\mathbf{k}}$ satisfy

$$u^2_{\mathbf{k}} = \frac{1}{2}\left[1 + \frac{\xi_{\mathbf{k}}}{\sqrt{\xi^2_{\mathbf{k}} + |\Delta_{\mathbf{k}}|^2}}\right],\ v^2_{\mathbf{k}} = \frac{1}{2}\left[1 - \frac{\xi_{\mathbf{k}}}{\sqrt{\xi^2_{\mathbf{k}} + |\Delta_{\mathbf{k}}|^2}}\right],$$

we can obtain the BCS ground state by solving the gap function self-consistently.

Multipolar FS deformation. We first illustrate with examples that the anisotropic Rydberg-dressed interaction can break the spherical symmetry of the FSs for noninteracting fermions. In Fig. 3(a1), we show the momentum distribution for $n = 25$ (i.e., the atoms are dressed to the $|25D_{5/2}, 5/2\rangle$ state), which displays a sharp edge at the FS. The FS is slightly deformed from a sphere, which is confirmed by a numerical fit of the FS based on the conventional mean-field solution (see the Supplemental Material, SM, for details [55]). This anisotropy results from the fact that the scattering of two atoms does not preserve each of their orbital angular momenta due to the anisotropic dressed interaction [59]. However, the difference of the momentum distribution from the interaction-free one, given by $\delta\tilde{\rho}(\mathbf{k}) = \tilde{\rho}(\mathbf{k}) - \tilde{\rho}_0(\mathbf{k})$, is marginal for the low-lying $n = 25$ state [Fig. 3(a2)].

The momentum distribution changes qualitatively with increasing principal quantum number n. For $n = 35$ [Fig. 3(b1)] and 55 [Fig. 3(c1)], the Fermi sea is depleted notably around k_F. Importantly, the momentum distributions become strongly anisotropic. To quantify the anisotropy of $\tilde{\rho}(\mathbf{k})$, we first evaluate its angular distribution by integrating over the radial part, $\chi(\theta_k) = 2\pi/N\int\tilde{\rho}(\mathbf{k})k^2dk$ with the normalization condition $\int_0^\pi \chi(\theta_k)\sin\theta_k d\theta_k = 1$. Here, the azimuthal angle ϕ_k has been integrated out straightly due to the cylindrical symmetry of $\tilde{\rho}(\mathbf{k})$. Then the angular function is expanded in terms of spherical harmonics, $\chi(\theta_k) = \sum_{l=0,2,4\ldots}\lambda_l Y_{l0}(\theta_k)$ where $\lambda_l = \int\chi(\theta_k)Y_{l0}(\theta_k)\sin\theta_k d\theta_k$ [55] is the coefficient of $\chi(\theta_k)$ projected to $Y_{l0}(\theta_k)$. Here, a nonvanishing λ_l ($l > 0$) means that the shape of the FS is not spherical. For parameters considered in this work, it is found that λ_l becomes negligible when $l > 6$.

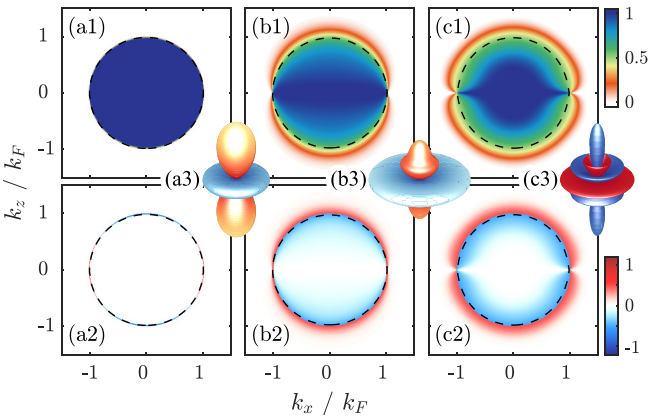

FIG. 3. State-dependent FS deformation. Density distribution in momentum space for (a1) $n = 25$ with $\bar{R} = 1.12$ μm, (b1) $n = 35$ with $\bar{R} = 2.08$ μm, and (c1) $n = 55$ with $\bar{R} = 4.77$ μm. The corresponding $\delta\tilde{\rho}(\mathbf{k})$ is given in panels (a2), (b2), and (c2). The dashed line in the first and second row is the fitted FS (see SM [55] for details), which locates the momentum where $\delta\tilde{\rho}(\mathbf{k}) \approx 0$. For $n = 25$, the deformation of the FS is described by the spherical harmonics $Y_{20}(\theta_k)$, shown in panel (a3). For $n = 35$ and 55, the FS deformation has complicated multipolar features, as shown in panels (b3) and (c3), respectively. Here $k_F = 2$ μm^{-1}, and other parameters are same with Fig. 1.

The main result of this work is that the shape of the FS involves multiple λ_l. As shown in Fig. 4(a), λ_2 is the only nonzero projection coefficient when $k_F\bar{R} < 3$ ($k_F \lesssim 0.6\bar{k}$) and assumes its maximal value around $k_F\bar{R} \approx 3$. In this region, we obtain a *dipolar deformation* ($l = 2$), where the FS is stretched in the k_z direction [Fig. 3(a3)], and becomes an ellipsoid. When $k_F\bar{R} > 3$, the amplitudes of λ_4 and λ_6 increase while the one for λ_2 decreases. In the region $3.5 \lesssim k_F\bar{R} \lesssim 5$, $|\lambda_4|$ and λ_6 become comparable to λ_2. In this *multipolar deformation* regime, mainly three spherical harmonics contribute to the FS: $Y_{20}(\theta_k)$, $Y_{40}(\theta_k)$, and $Y_{60}(\theta_k)$ [Fig. 3(b3)]. When further increasing $k_F\bar{R} > 6$, the value of all λ_l decreases and saturates. As $|\lambda_4| > |\lambda_6| > |\lambda_2|$, this yields a FS deformation significantly different [Fig. 3(c3)] from the one shown in Fig. 3(a3).

The depletion of the momentum density becomes significant when the multipolar deformation is present. This leads to an increase of the variance $\text{Var}(\tilde{\rho}) = \sum_{\mathbf{k}}[\tilde{\rho}(\mathbf{k}) - \tilde{\rho}_0(\mathbf{k})]^2/\rho$ of the momentum distribution, as shown in the inset of Fig. 4(b). However, when $n < 30$, the variance is small and increases only slowly with n. When $n > 30$, it increases rapidly and saturates gradually, where the deformation is given mainly by the λ_6 term [Fig. 4(a)].

Scaling in the dipolar deformation regime. The value of λ_2, which parametrizes the FS deformation, follows a power-law scaling with respect to the system parameters, such as the interaction strength V_0, the density of atoms ρ, and the interaction length $\bar{R}$. When λ_2 dominates, we find that the density distribution changes rapidly at the FS which gives rise to a modified Fermi momentum $\mathbf{k}'_F$ [Fig. 3(a1)]. This deformation

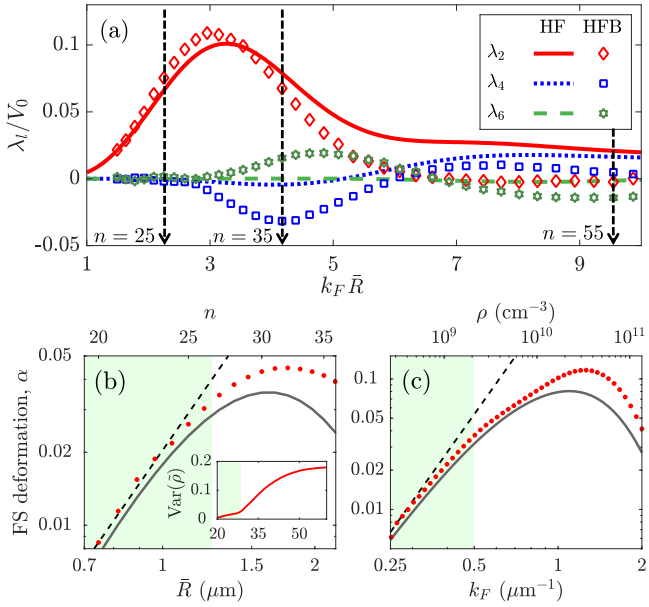

FIG. 4. Characterization of the multipolar FS. (a) The projection coefficient λ_j (diamond, square, star) and λ'_j (solid, dotted, dashed) based on the HFB and HF calculation. In the calculation, we vary $\bar{R}$ (through n) and fix $k_F = 2\ \mu\mathrm{m}^{-1}$. λ_2 dominates when $k_F\bar{R} < 3$ ($n < 30$). λ_4 and λ_6 become important when $k_F\bar{R} > 3$, where the multipolar FS deformation emerges. When $k_F\bar{R} \lesssim 3$, the deformation of the FS can also be characterized by its ellipticity, $\alpha = 1 - \mathbf{k}_F(0)/\mathbf{k}_F(\pi/2)$. In panels (b) and (c), we show the ellipticity by changing the soft-core radius $\bar{R}$ (n) and k_F (ρ), respectively. When λ_2 dominates, one finds $\alpha \approx 3\sqrt{5/\pi}\lambda_2/4$, establishing a relation of the ellipticity and λ_2. The numerical data (dots) and perturbation results (solid) follow the power-law scaling well in the shaded area. The inset in panel (b) shows the variance of the density distribution $\tilde{\rho}(\mathbf{k})$. (b) $k_F = 2\ \mu\mathrm{m}^{-1}$ and (c) $n = 35$. Other parameters are same as in Fig. 1.

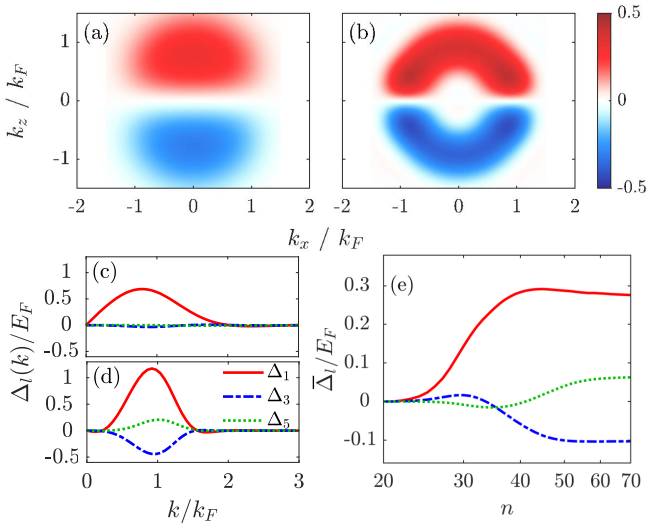

FIG. 5. Cooper pairs of multiple partial waves. Gap functions $\Delta(\mathbf{k})$ for (a) $n = 35$ and (b) $n = 55$. The projection of $\Delta(\mathbf{k})$ to the spherical harmonics Y_{l0} (l odd) for (b) $n = 35$ and (c) $n = 55$, respectively. For panel (c), $n = 35$, the gap function is occupied by the p-wave component. For panel (d), $n = 55$, it turns out that f-wave ($l = 3$) and h-wave ($l = 5$) pairing become important as well. (e) The population of various pair states as a function of quantum number n. Note that f- and h-wave pairing are non-negligible when $n > 40$. Other parameters are the same as those in Figs. 4(b) and 4(c), respectively.

is quantified by the deviation of $\mathbf{k}'_F$ from k_F, $\delta\mathbf{k}_F = \mathbf{k}'_F - k_F\vec{\mathbf{n}}$, where $\vec{\mathbf{n}}$ is the unit vector parallel to $\mathbf{k}'_F$. As pairing is not important here, $\delta\mathbf{k}_F$ can be evaluated from the Hartree-Fock energy [60,61]

$$\frac{\delta\mathbf{k}_F}{k_F} \approx \frac{1}{2E_F}\int d^3\mathbf{q}\tilde{V}(\mathbf{k}'_F - \mathbf{q})\tilde{\rho}(\mathbf{q}). \tag{7}$$

Assuming $\tilde{\rho}(\mathbf{q}) \approx \tilde{\rho}_0(\mathbf{q})$ and projecting $\delta\mathbf{k}_F$ onto spherical harmonics, this yields

$$\frac{\delta\mathbf{k}_F}{k_F} \approx \frac{4\pi}{3}\sum_{l=2,4,6}\lambda_l Y_{l0}(\theta_k), \tag{8}$$

with $\lambda_l = 3/(8\pi E_F)\int_0^\infty F_l(k/k_F\bar{R})G_l(k)dk$ being the approximate projection coefficient. Here, we have defined $F_l(k) = \int_0^\pi Y_{l0}(\theta_k)V(k\bar{R},\theta_k)\sin\theta_k\mathrm{d}\theta_k$ and $G_l(k) = 4i^l x j_1(k) j_l(k)$, where $j_l(k)$ is the spherical Bessel function of the first kind (see the SM [55]).

As shown in Fig. 4(a), the coefficient λ_2, obtained from the perturbative calculation agrees well with the full-numerical method up to $k_F\bar{R} \approx 3$. In this region, we can make a Taylor expansion of λ_2 in terms of $k_F\bar{R}$, whose leading term is $\lambda_2 \propto V_0(k_F\bar{R})^5/E_F$ [55]. This results in the power law relations $\lambda_2 \propto \bar{R}^3, n^{11/2}, k_F^3$. This scaling matches with the numerical calculations when $k_F\bar{R}$ is small, as shown by the shaded area in Figs. 4(b) and 4(c). Experimentally, the predicted scaling can be measured by tuning the atomic density (k_F) and laser parameters (n and δ) jointly or separately, which is useful in exploring the FS deformation and the dressed interaction experimentally. Finally, we note that the peak at $k_F\bar{R} \approx 3$ can also be explained within the perturbative treatment pursued here: $F_2[k/(k_F\bar{R})]$ has a single peak located at $k = k_F\bar{R}$, and $G_2(k)$ oscillates with k, as discussed in the SM [55]. We thus obtain the maximal λ_2 when the peaks of $F_2(k)$ and $G_2(k)$ coincide at $k_F\bar{R} \approx 3$.

Cooper pairing in the multipolar deformation regime. In the HFB approach, the gap function $\Delta(\mathbf{k})$ serves as an order parameter of superfluidity. Here the superfluid is formed by Cooper pairs of two fermionic atoms with opposite momenta [21,59]. In Fig. 5(a), we show the distribution of the gap function $\Delta(\mathbf{k})$ for $n = 35$. It is nonzero in a wide region around the FS where the momentum density differs drastically from the interaction-free Fermi sea [Fig. 3(b1)]. Here an antisymmetry of the gap function is observed along the k_z axis. For $n = 55$ [Fig. 5(b)], the pair distribution becomes more confined around the FS, and its peak value increases [Fig. 3(c1)].

To gain further insights of the pairing, we expand the gap function into partial waves, $\Delta(\mathbf{k}) = \sum_l \Delta_l(k)Y_{lm}(\theta_k)$ with $\Delta_l(k) = \int \Delta(\mathbf{k})Y_{lm}(\theta_k,\phi_\mathbf{k})d\Omega_\mathbf{k}$ being the l-wave pair state (l is an odd integer) [59]. As shown in Fig. 5(c), p-wave pairing is dominant when $n = 35$. Importantly, new pairing states emerge when the FS is deformed strongly. As depicted in

Fig. 5(d), f-wave ($l = 3$) and h-wave ($l = 5$) pairing, together with p-wave pairing, are found when $n = 55$. A systematic study shows that the population of the Cooper pairs can be enhanced by dressing to higher (more strongly interacting) Rydberg states. In Fig. 5(e), the total population of individual pair states, $\bar{\Delta}_l = \int d^3\mathbf{k}\Delta_l(\mathbf{k})$, is shown. When n increases, the occupation of p-, f-, and h-wave pairs also increases. In particular, considerable f- and h-wave populations are obtained when $n > 40$.

Discussion and outlook. The quantum simulation of p- and f-wave pairing with ultracold atoms has attracted much attention due to their importance in understanding superfluidity in ^{3}He-A [51], ^{3}He-B phase [52], and unconventional superconductors [53]. It has been shown that p-wave pairing can be realized with ultracold fermions with the dipolar interaction [21,62–65] or isotropic dressed interaction in three dimensions [46]. However, f-wave pairing can only occur in 2D under extra restricted conditions, including Bose-Fermi mixed interactions [66,67], excited bands [68], and repulsive Rydberg-dressed interactions [49,50]. Our results show that an anisotropic Rydberg-dressed interaction allows to achieve such unconventional pairing states in three dimensions (3D). Moreover, it even provides access to the h-wave pairing channel.

Such h-wave pairing has not been thoroughly studied and is certainly worth further exploration. The anisotropic and attractive dressed interaction opens further opportunities to probe novel phases, such as the nematic phase [2], topological superfluid [64,69,70], and supersolid phases [71,72], as well as to probe nonequilibrium dynamics driven by long-range anisotropic interactions [45,73]. Finally, we remark that anisotropic but repulsive interactions [55] can be obtained in the Rydberg dressing of ^{39}K atoms [74]. Such repulsive interaction allows for probing the Kohn-Luttinger mechanism [75–77].

Acknowledgments. We are thankful for useful discussions with Yongqiang Li, Vijay Shenoy, S. Kumar Mallavarapu, and Gary McCormack. Y.Z. acknowledges support from National Natural Science Foundation of China (Grant No. 12088101) and NSAF (Grant No. U1930403). W.L. acknowledges support from the EPSRC through Grant No. EP/R04340X/1 via the QuantERA project "ERyQSenS," the UKIERI-UGC Thematic Partnership (IND/CONT/G/16-17/73), and the Royal Society through the International Exchanges Cost Share Award No. IEC\NSFC\181078. R.N. acknowledges DST-SERB for Swarnajayanti Fellowship File No. SB/SJF/2020-21/19. I.L. acknowledges support from the "Wissenschaftler Rückkehrprogramm GSO/CZS" of the Carl-Zeiss-Stiftung and the German Scholars Organization e.V., as well as the Deutsche Forschungsgemeinschaft through SPP 1929 (GiRyd), Grant No. 428276754, and the "Internationale Spitzenforschung" program of the BW Foundation. We are grateful for access to the Augusta High Performance Computing Facility at the University of Nottingham.

[1] G. Baym and C. Pethick, *Landau Fermi-Liquid Theory: Concepts and Applications* (John Wiley & Sons, New York, 2008).

[2] S. A. Kivelson, E. Fradkin, and V. J. Emery, Electronic liquid-crystal phases of a doped Mott insulator, Nature (London) **393**, 550 (1998).

[3] I. I. Pomeranchuk, On the stability of a Fermi liquid, Sov. Phys. JETP **8**, 361 (1959).

[4] S. Giorgini, L. P. Pitaevskii, and S. Stringari, Theory of ultracold atomic Fermi gases, Rev. Mod. Phys. **80**, 1215 (2008).

[5] T. E. Drake, Y. Sagi, R. Paudel, J. T. Stewart, J. P. Gaebler, and D. S. Jin, Direct observation of the Fermi surface in an ultracold atomic gas, Phys. Rev. A **86**, 031601(R) (2012).

[6] B. Mukherjee, Z. Yan, P. B. Patel, Z. Hadzibabic, T. Yefsah, J. Struck, and M. W. Zwierlein, Homogeneous Atomic Fermi Gases, Phys. Rev. Lett. **118**, 123401 (2017).

[7] M. Marinescu and L. You, Controlling Atom-Atom Interaction at Ultralow Temperatures By DC Electric Fields, Phys. Rev. Lett. **81**, 4596 (1998).

[8] K.-K. Ni, S. Ospelkaus, M. H. G. de Miranda, A. Pe'er, B. Neyenhuis, J. J. Zirbel, S. Kotochigova, P. S. Julienne, D. S. Jin, and J. Ye, A high phase-space-density gas of polar molecules, Science **322**, 231 (2008).

[9] M. Lu, N. Q. Burdick, and B. L. Lev, Quantum Degenerate Dipolar Fermi Gas, Phys. Rev. Lett. **108**, 215301 (2012).

[10] M. A. Baranov, M. Dalmonte, G. Pupillo, and P. Zoller, Condensed matter theory of dipolar quantum gases, Chem. Rev. **112**, 5012 (2012).

[11] T. Shi, S.-H. Zou, H. Hu, C.-P. Sun, and S. Yi, Ultracold Fermi Gases with Resonant Dipole-Dipole Interaction, Phys. Rev. Lett. **110**, 045301 (2013).

[12] S. Baier, D. Petter, J. H. Becher, A. Patscheider, G. Natale, L. Chomaz, M. J. Mark, and F. Ferlaino, Realization of a Strongly Interacting Fermi Gas of Dipolar Atoms, Phys. Rev. Lett. **121**, 093602 (2018).

[13] A. Trautmann, P. Ilzhöfer, G. Durastante, C. Politi, M. Sohmen, M. J. Mark, and F. Ferlaino, Dipolar Quantum Mixtures of Erbium and Dysprosium Atoms, Phys. Rev. Lett. **121**, 213601 (2018).

[14] T. Miyakawa, T. Sogo, and H. Pu, Phase-space deformation of a trapped dipolar Fermi gas, Phys. Rev. A **77**, 061603(R) (2008).

[15] G. M. Bruun and E. Taylor, Quantum Phases of a Two-Dimensional Dipolar Fermi Gas, Phys. Rev. Lett. **101**, 245301 (2008).

[16] B. M. Fregoso and E. Fradkin, Ferronematic Ground State of the Dilute Dipolar Fermi Gas, Phys. Rev. Lett. **103**, 205301 (2009).

[17] J.-N. Zhang and S. Yi, Fermi surface of a trapped dipolar Fermi gas, Phys. Rev. A **80**, 053614 (2009).

[18] T. Sogo, L. He, T. Miyakawa, S. Yi, H. Lu, and H. Pu, Dynamical properties of dipolar Fermi gases, New J. Phys. **11**, 055017 (2009).

[19] Y. Yamaguchi, T. Sogo, T. Ito, and T. Miyakawa, Density-wave instability in a two-dimensional dipolar Fermi gas, Phys. Rev. A **82**, 013643 (2010).

[20] D. Baillie and P. B. Blakie, Thermodynamics and coherence of a trapped dipolar Fermi gas, Phys. Rev. A **82**, 033605 (2010).

[21] C. Zhao, L. Jiang, X. Liu, W. M. Liu, X. Zou, and H. Pu, Hartree-Fock-Bogoliubov theory of dipolar Fermi gases, Phys. Rev. A **81**, 063642 (2010).

[22] F. Wächtler, A. R. P. Lima, and A. Pelster, Low-lying excitation modes of trapped dipolar Fermi gases: From the collisionless to the hydrodynamic regime, Phys. Rev. A **96**, 043608 (2017).

[23] K. Aikawa, S. Baier, A. Frisch, M. Mark, C. Ravensbergen, and F. Ferlaino, Observation of Fermi surface deformation in a dipolar quantum gas, Science **345**, 1484 (2014).

[24] I. Bouchoule and K. Mølmer, Spin squeezing of atoms by the dipole interaction in virtually excited Rydberg states, Phys. Rev. A **65**, 041803(R) (2002).

[25] N. Henkel, R. Nath, and T. Pohl, Three-Dimensional Roton Excitations and Supersolid Formation in Rydberg-Excited Bose-Einstein Condensates, Phys. Rev. Lett. **104**, 195302 (2010).

[26] G. Pupillo, A. Micheli, M. Boninsegni, I. Lesanovsky, and P. Zoller, Strongly correlated Gases of Rydberg-Dressed Atoms: Quantum and Classical Dynamics, Phys. Rev. Lett. **104**, 223002 (2010).

[27] J. Honer, H. Weimer, T. Pfau, and H. P. Büchler, Collective Many-Body Interaction in Rydberg Dressed Atoms, Phys. Rev. Lett. **105**, 160404 (2010).

[28] F. Cinti, P. Jain, M. Boninsegni, A. Micheli, P. Zoller, and G. Pupillo, Supersolid Droplet Crystal in a Dipole-Blockaded Gas, Phys. Rev. Lett. **105**, 135301 (2010).

[29] W. Li, L. Hamadeh, and I. Lesanovsky, Probing the interaction between Rydberg-dressed atoms through interference, Phys. Rev. A **85**, 053615 (2012).

[30] M. Saffman, T. G. Walker, and K. Mølmer, Quantum information with Rydberg atoms, Rev. Mod. Phys. **82**, 2313 (2010).

[31] E. Guardado-Sanchez, P. T. Brown, D. Mitra, T. Devakul, D. A. Huse, P. Schauß, and W. S. Bakr, Probing the Quench Dynamics of Antiferromagnetic Correlations in a 2D Quantum Ising Spin System, Phys. Rev. X **8**, 021069 (2018).

[32] S. de Léséleuc, V. Lienhard, P. Scholl, D. Barredo, S. Weber, N. Lang, H. P. Büchler, T. Lahaye, and A. Browaeys, Observation of a symmetry-protected topological phase of interacting bosons with Rydberg atoms, Science **365**, 775 (2019).

[33] A. W. Glaetzle, M. Dalmonte, R. Nath, C. Gross, I. Bloch, and P. Zoller, Designing Frustrated Quantum Magnets with Laser-Dressed Rydberg Atoms, Phys. Rev. Lett. **114**, 173002 (2015).

[34] R. M. W. van Bijnen and T. Pohl, Quantum Magnetism and Topological Ordering Via Rydberg Dressing Near Förster Resonances, Phys. Rev. Lett. **114**, 243002 (2015).

[35] F. Cinti, T. Macrì, W. Lechner, G. Pupillo, and T. Pohl, Defect-induced supersolidity with soft-core bosons, Nat. Commun. **5**, 3235 (2014).

[36] H. Schempp, G. Günter, S. Wüster, M. Weidemüller, and S. Whitlock, Correlated Exciton Transport in Rydberg-Dressed-Atom Spin Chains, Phys. Rev. Lett. **115**, 093002 (2015).

[37] C.-H. Hsueh, C.-W. Wang, and W.-C. Wu, Vortex structures in a rotating Rydberg-dressed Bose-Einstein condensate with the Lee-Huang-Yang correction, Phys. Rev. A **102**, 063307 (2020).

[38] Y. Zhou, Y. Li, R. Nath, and W. Li, Quench dynamics of Rydberg-dressed bosons on two-dimensional square lattices, Phys. Rev. A **101**, 013427 (2020).

[39] J. Zeiher, R. van Bijnen, P. Schauß, S. Hild, J.-y. Choi, T. Pohl, I. Bloch, and C. Gross, Many-body interferometry of a Rydberg-dressed spin lattice, Nat. Phys. **12**, 1095 (2016).

[40] J. Zeiher, J.-y. Choi, A. Rubio-Abadal, T. Pohl, R. van Bijnen, I. Bloch, and C. Gross, Coherent Many-Body Spin Dynamics in a Long-Range Interacting Ising Chain, Phys. Rev. X **7**, 041063 (2017).

[41] V. Borish, O. Marković, J. A. Hines, S. V. Rajagopal, and M. Schleier-Smith, Transverse-Field Ising Dynamics in a Rydberg-Dressed Atomic Gas, Phys. Rev. Lett. **124**, 063601 (2020).

[42] Y. Li, A. Geißler, W. Hofstetter, and W. Li, Supersolidity of lattice bosons immersed in strongly correlated Rydberg dressed atoms, Phys. Rev. A **97**, 023619 (2018).

[43] R. Mukherjee, C. Ates, W. Li, and S. Wüster, Phase-Imprinting of Bose-Einstein Condensates with Rydberg Impurities, Phys. Rev. Lett. **115**, 040401 (2015).

[44] Y. Li, H. Cai, D.-w. Wang, L. Li, J. Yuan, and W. Li, Many-Body Chiral Edge Currents and Sliding Phases of Atomic Spin Waves in Momentum-Space Lattice, Phys. Rev. Lett. **124**, 140401 (2020).

[45] E. Guardado-Sanchez, B. M. Spar, P. Schauss, R. Belyansky, J. T. Young, P. Bienias, A. V. Gorshkov, T. Iadecola, and W. S. Bakr, Quench Dynamics of a Fermi Gas with Strong Nonlocal Interactions, Phys. Rev. X **11**, 021036 (2021).

[46] B. Xiong, H. H. Jen, and D.-W. Wang, Topological superfluid by blockade effects in a Rydberg-dressed Fermi gas, Phys. Rev. A **90**, 013631 (2014).

[47] X. Li and S. D. Sarma, Exotic topological density waves in cold atomic Rydberg-dressed fermions, Nat. Commun. **6**, 7137 (2015).

[48] W.-H. Li, T.-C. Hsieh, C.-Y. Mou, and D.-W. Wang, Emergence of a Metallic Quantum Solid Phase in a Rydberg-Dressed Fermi Gas, Phys. Rev. Lett. **117**, 035301 (2016).

[49] R. Khasseh, S. H. Abedinpour, and B. Tanatar, Phase diagram and dynamics of Rydberg-dressed fermions in two dimensions, Phys. Rev. A **96**, 053611 (2017).

[50] A. Keleş, E. Zhao, and X. Li, f-wave superfluidity from repulsive interaction in Rydberg-dressed Fermi gas, Phys. Rev. A **101**, 023624 (2020).

[51] U. E. Israelsson, B. C. Crooker, H. M. Bozler, and C. M. Gould, f-Wave Effects in Superfluid ^{3}He-A, Phys. Rev. Lett. **56**, 2383 (1986).

[52] J. P. Davis, J. Pollanen, H. Choi, J. A. Sauls, and W. P. Halperin, Discovery of an excited pair state in superfluid ^{3}He, Nat. Phys. **4**, 571 (2008).

[53] G. R. Stewart, Unconventional superconductivity, Adv. Phys. **66**, 75 (2017).

[54] A. A. Kamenski, N. L. Manakov, S. N. Mokhnenko, and V. D. Ovsiannikov, Energy of van der Waals and dipole-dipole interactions between atoms in Rydberg states, Phys. Rev. A **96**, 032716 (2017).

[55] See Supplemental Material at http://link.aps.org/supplemental/10.1103/PhysRevA.104.L061302 for additional details on the van der Waals interaction and HFB approximation, which also includes Refs. [56,78–82].

[56] J. E. Johnson and S. L. Rolston, Interactions between Rydberg-dressed atoms, Phys. Rev. A **82**, 033412 (2010).

[57] C. Cohen-Tannoudji, J. Dupont-Roc, and G. Grynberg, Nonperturbative calculation of transition amplitudes, in *Atom-Photon Interactions: Basic Process and Appilcations* (John Wiley & Sons, New York, 1998), Chap. 3, pp. 165–255.

[58] P. Ring and P. Schuck, *The Nuclear Many-Body Problem* (Springer-Verlag, Berlin, 1980).

[59] L. You and M. Marinescu, Prospects for p-wave paired Bardeen-Cooper-Schrieffer states of fermionic atoms, Phys. Rev. A **60**, 2324 (1999).

[60] C.-K. Chan, C. Wu, W.-C. Lee, and S. Das Sarma, Anisotropic-Fermi-liquid theory of ultracold fermionic polar molecules: Landau parameters and collective modes, Phys. Rev. A **81**, 023602 (2010).

[61] S. Ronen and J. L. Bohn, Zero sound in dipolar Fermi gases, Phys. Rev. A **81**, 033601 (2010).

[62] T.-L. Ho and R. B. Diener, Fermion Superfluids of Nonzero Orbital Angular Momentum Near Resonance, Phys. Rev. Lett. **94**, 090402 (2005).

[63] C.-H. Cheng and S.-K. Yip, Pairing symmetry in an anisotropic Fermi superfluid under a p-wave Feshbach resonance, Phys. Rev. B **73**, 064517 (2006).

[64] N. R. Cooper and G. V. Shlyapnikov, Stable Topological Superfluid Phase of Ultracold Polar Fermionic Molecules, Phys. Rev. Lett. **103**, 155302 (2009).

[65] A. K. Fedorov, S. I. Matveenko, V. I. Yudson, and G. V. Shlyapnikov, Novel p-wave superfluids of fermionic polar molecules, Sci. Rep. **6**, 27448 (2016).

[66] W.-C. Lee, C. Wu, and S. Das Sarma, f-wave pairing of cold atoms in optical lattices, Phys. Rev. A **82**, 053611 (2010).

[67] L. Mathey, S.-W. Tsai, and A. H. Castro Neto, Exotic superconducting phases of ultracold atom mixtures on triangular lattices, Phys. Rev. B **75**, 174516 (2007).

[68] H.-H. Hung, W.-C. Lee, and C. Wu, Frustrated Cooper pairing and f-wave supersolidity in cold-atom optical lattices, Phys. Rev. B **83**, 144506 (2011).

[69] B. Liu and L. Yin, Topological $p_x + ip_y$ superfluid phase of a dipolar Fermi gas in a two-dimensional optical lattice, Phys. Rev. A **86**, 031603(R) (2012).

[70] B. Liu, X. Li, L. Yin, and W. V. Liu, Weyl Superfluidity in a Three-Dimensional Dipolar Fermi Gas, Phys. Rev. Lett. **114**, 045302 (2015).

[71] A.-L. Gadsbølle and G. M. Bruun, Harmonically trapped dipolar fermions in a two-dimensional square lattice, Phys. Rev. A **85**, 021604(R) (2012).

[72] T.-S. Zeng and L. Yin, Supersolidity of a dipolar Fermi gas in a cubic optical lattice, Phys. Rev. B **89**, 174511 (2014).

[73] N. Nessi, A. Iucci, and M. A. Cazalilla, Quantum Quench and Prethermalization Dynamics in a Two-Dimensional Fermi Gas with Long-Range Interactions, Phys. Rev. Lett. **113**, 210402 (2014).

[74] A. Arias, G. Lochead, T. M. Wintermantel, S. Helmrich, and S. Whitlock, Realization of a Rydberg-Dressed Ramsey Interferometer and Electrometer, Phys. Rev. Lett. **122**, 053601 (2019).

[75] D. Shechtman, I. Blech, D. Gratias, and J. W. Cahn, Metallic Phase with Long-Range Orientational Order and No Translational Symmetry, Phys. Rev. Lett. **53**, 1951 (1984).

[76] S. Maiti and A. V. Chubukov, Superconductivity from repulsive interaction, in *Lectures on the Physics of Strongly Correlated Systems XVII: Seventeenth Training Course in the Physics of Strongly Correlated Systems*, edited by A.Avella and F. Mancini, AIP Conf. Proc. No. 1550 (AIP, New York, 2013), p. 3.

[77] Y. Cao, Y. Zhang, Y.-B. Liu, C.-C. Liu, W.-Q. Chen, and F. Yang, Kohn-Luttinger Mechanism Driven Exotic Topological Superconductivity on the Penrose Lattice, Phys. Rev. Lett. **125**, 017002 (2020).

[78] N. Šibalić, J. Pritchard, C. Adams, and K. Weatherill, ARC: An open-source library for calculating properties of alkali Rydberg atoms, Comput. Phys. Commun. **220**, 319 (2017).

[79] E. Robertson, N. Šibalić, R. Potvliege, and M. Jones, ARC 3.0: An expanded PYTHON toolbox for atomic physics calculations, Comput. Phys. Commun. **261**, 107814 (2021).

[80] Z. Lan, J. Minář, E. Levi, W. Li, and I. Lesanovsky, Emergent Devil's Staircase Without Particle-Hole Symmetry in Rydberg Quantum Gases with competing attractive and repulsive interactions, Phys. Rev. Lett. **115**, 203001 (2015).

[81] Z. Lan, I. Lesanovsky, and W. Li, Devil's staircases without particle-hole symmetry, Phys. Rev. B **97**, 075117 (2018).

[82] N. D. Woods, M. C. Payne, and P. J. Hasnip, Computing the self-consistent field in Kohn-Sham density functional theory, J. Phys.: Condens. Matter **31**, 453001 (2019).